



Anomalous glass transition behavior in Cu–Zr–Sn alloy system

E.S. Park^{a,*}, M. Ohnuma^b, D.H. Kim^c

^a Research Institute of Advanced Materials, Department of Materials Science and Engineering, Seoul National University, Seoul 151-744, Republic of Korea

^b National Institute for Material Science, 1-2-1 Sengen, Tsukuba 305-0047, Japan

^c Center for Non-crystalline Materials, Yonsei University, Seoul 120-749, Republic of Korea

ARTICLE INFO

Article history:

Received 2 August 2010

Received in revised form 13 January 2011

Accepted 14 January 2011

Available online 22 January 2011

Keywords:

Metallic glass

Anomalous glass transition

SAXS analysis

Quenched-in nuclei

TTT diagram

ABSTRACT

We discuss the effect of Sn addition on anomalous glass transition behavior in Cu–Zr bulk-forming metallic glasses. We found that an unusual endothermic reaction in Cu₅₅Zr₄₀Sn₅ ribbon can originate from the growth reaction of quenched-in nuclei from 0.4 nm to 3.7 nm in the supercooled liquid region. This anomalous devitrification may prove useful for the synthesis of a novel composite with uniform atomic/nanometer scale heterogeneity modulated by controlling cooling rate as well as by tailoring alloy composition.

© 2011 Elsevier B.V. All rights reserved.

1. Introduction

Bulk-forming metallic glasses (BMGs) are of interest not only in themselves but also because they are the precursors of useful glass–nanocrystal composites, obtained by devitrification [1]. Such a microstructure manipulation may be achieved by a suitable annealing of amorphous alloys as well as an appropriate cooling history.

The presence of the glass → liquid transition on heating is clear evidence for a high thermal stability of supercooled liquid and thereby amorphous states, and appears to be directly connected with the thermodynamic property of glass-forming liquid [2]. While most of metallic glasses exhibit a single endothermic reaction at the glass transition temperature (T_g), anomalous glass transition behavior such as an additional endothermic reaction has been reported in some limited cases [3–8]. However, this abnormal behavior of supercooled liquid region (SCLR, $\Delta T = T_x - T_g$) may be useful in tailoring properties obtained by unique devitrification such as selective partial devitrification [5].

It is well known that binary Cu–Zr metallic glasses exhibit a large SCLR of over 40 K in the composition range of 35–70 at.% Zr, and the BMG rods with diameters of 1–2 mm are formed in the composition range of 35–55 at.% Zr, indicating that the binary Cu–Zr alloys have high stabilization of SCLR and high glass-forming ability [9]. This result strongly suggests that the SCLR may be modified by appro-

priately introducing an additional alloying element. For instance, Inoue et al. reported that the SCLR increases over 70 K with minor addition of Al or Ag [9,10] and Park et al. reported that apparent double glass transition behavior occurs with a minor addition of Be [7]. However, there is little documentation for the anomalous behavior of SCLR in Cu–Zr BMG. In the present study, we further explore the manipulation of SCLR in Cu–Zr BMG system and, in particular, study the effect of Sn addition on the thermal stability of supercooled liquid in a series of Cu_{60-x}Zr₄₀Sn_x alloys. In our experiments, a unique endothermic reaction between the first and the second crystallization was detected in Cu₅₅Zr₄₀Sn₅ ribbon. It can be understood that the anomalous glass transition behavior results from the growth reaction of quenched-in nuclei from 0.4 nm to 3.7 nm in the SCLR, which is closely related to strong affinity (Zr–Sn: –172 kJ/mol) and large size mismatch among constituent elements.

2. Experimental

Alloy ingots with compositions of Cu_{60-x}Zr₄₀Sn_x ($x=0, 1, 3, 5, 7.5$ at.%) were produced by arc melting high purity elements (>99.9%) under a Ti-gettered argon atmosphere in a water cooled copper crucible. Rapidly solidified specimens were prepared by re-melting appropriate amounts of the alloys in quartz tubes, and ejecting with an over-pressure of 50 kPa through a nozzle onto a copper wheel rotating with a surface velocity of 40 m/s.

The structures of the samples were examined preliminarily by X-ray diffraction (XRD; Rigaku CN2301) using monochromatic Cu K α radiation for a 2θ range of 10–90°. High-resolution neutron diffraction (HRND) experiments were performed using the intense pulse neutron source of the High-flux Advanced Neutron Application Reactor (HANARO) at the Korea Atomic Energy Research Institute. The HRND data were obtained in a 2θ range of 0–160° using neutrons of wavelengths $\lambda=0.1835$ nm by 32 monitors with a scanning speed of 0.014°/s.

* Corresponding author. Tel.: +82 2 880 7221; fax: +82 2 883 8197.

E-mail address: espark@snu.ac.kr (E.S. Park).

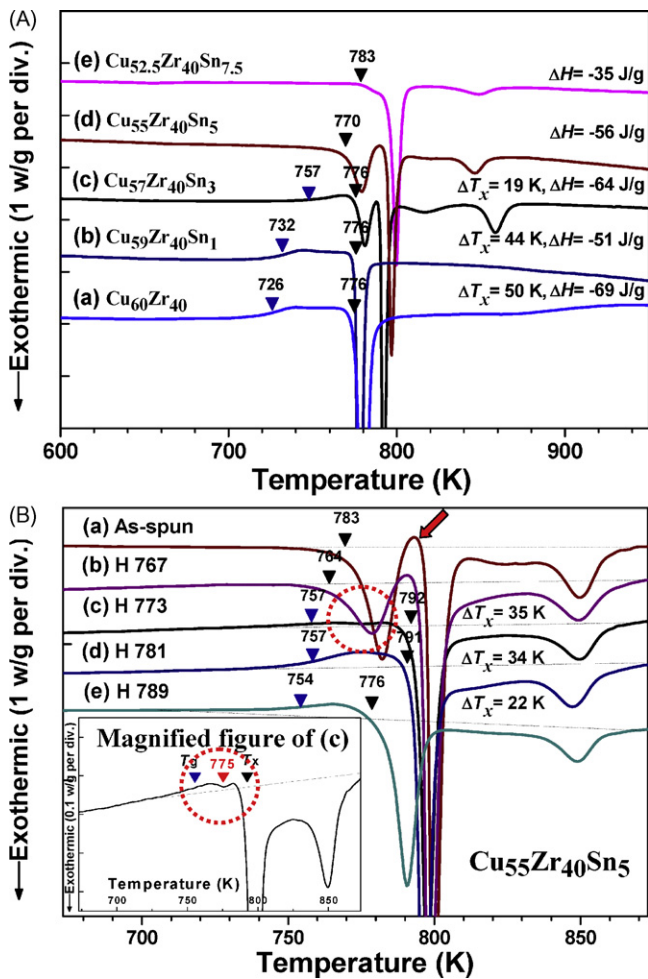


Fig. 1. (A) DSC traces obtained from (a–e) as-spun $\text{Cu}_{60-x}\text{Zr}_{40}\text{Sn}_x$ ($x=0, 1, 3, 5, 7.5$ at.%) ribbons. (B) DSC traces obtained from as-spun $\text{Cu}_{55}\text{Zr}_{40}\text{Sn}_5$ ribbon in (a) as-quenched state and after annealing up to: (b) 767 K, (c) 773 K, (d) 781 K, and (e) 789 K. The inset figure shows a magnified figure of curve (c).

The microstructures of the samples were examined using a high resolution transmission electron microscope (HRTEM; JEOL 4010, 400 kV). The thin foil specimens for HRTEM were prepared by Ar ion milling using Gatan, Model 600 at 2.6 keV and -5 mA with liquid nitrogen cooling. Thermal analysis was carried out by differential scanning calorimetry (DSC; Perkin Elmer DSC7). For detailed analysis on the local atomic structure, small-angle X-ray scattering was performed on $20\ \mu\text{m}$ thick ribbons using a RIGAKU PSAX-3S with pinhole collimation. A q range of $0.1\text{--}6\ \text{nm}^{-1}$ was covered with Mo $K\alpha$ radiation and the sample to detector distance was 970 mm. A two-dimensional position sensitive detector (Bruker Hi-star) was used in this study.

3. Results and discussion

The formation of an amorphous phase was confirmed from the broad halos of XRD profiles in as-spun $\text{Cu}_{60-x}\text{Zr}_{40}\text{Sn}_x$ ($x=0, 1, 3, 5, 7.5$ at.%) ribbons (not shown). Fig. 1A shows DSC traces obtained from as-spun $\text{Cu}_{60-x}\text{Zr}_{40}\text{Sn}_x$ ($x=0, 1, 3, 5, 7.5$ at.%) ribbons during continuous heating with a heating rate of $0.667\ \text{K/s}$. Each DSC trace shows one or two exothermic peaks, corresponding to the crystallization of the amorphous structure. When we increased Sn content, the second exothermic peak became separated from the first peak, which means that Sn addition resulted in different crystallization behaviors. The T_g and the T_x are marked by arrows in the DSC traces. The T_g of as-spun $\text{Cu}_{60-x}\text{Zr}_{40}\text{Sn}_x$ alloys increased from $726\ \text{K}$ at $x=0$ to $757\ \text{K}$ at $x=3$, then could not be observed above $x>3$. The T_x remained approximately the same ($776 \pm 7\ \text{K}$) regardless of the Sn content. Thus, the SCLR decreased from $50\ \text{K}$ at $x=0$ to $0\ \text{K}$ at $x=5$. Interestingly, in the case of the alloy with Sn 5 at.%, although

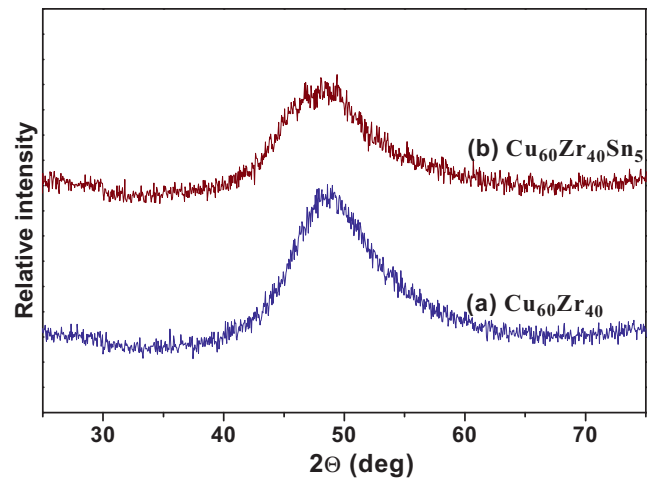


Fig. 2. HRND profiles obtained from the as-spun (a) $\text{Cu}_{60}\text{Zr}_{40}$ and (b) $\text{Cu}_{55}\text{Zr}_{40}\text{Sn}_5$ ribbons.

the alloy did not show an endothermic reaction for a glass transition before crystallization, a unique endothermic reaction between the first and the second exothermic peak was observed as marked in Fig. 1B(a). To understand this anomalous endothermic reaction, DSC traces were obtained from the samples pre-annealed up to $767\ \text{K}$, $773\ \text{K}$, $781\ \text{K}$ and $789\ \text{K}$ during $10\ \text{s}$ after continuous heating with a rate of $0.667\ \text{K/s}$ as shown in Fig. 1B(b–d), respectively. With an increase in the pre-annealing temperature, the exothermic peak related with the first crystallization decreased and, interestingly, an endothermic reaction related with supercooled liquid appeared as shown in Fig. 1B(c–e). The inset figure in Fig. 1B clearly shows T_g with a diminishing exothermic reaction of the first crystallization. This result leads us to form the hypotheses that two amorphous phases formed during solidification coexist in the as-spun ribbon or that remaining glass after the first crystallization exhibits strong resistance to crystallization.

To evaluate these hypotheses, intensive structural analyses were performed using HRND and HRTEM. Fig. 2 shows the HRND profiles obtained from the as-spun (a) $\text{Cu}_{60}\text{Zr}_{40}$ and (b) $\text{Cu}_{55}\text{Zr}_{40}\text{Sn}_5$ ribbons. The HRND profiles of as-spun $\text{Cu}_{60}\text{Zr}_{40}$ (Fig. 2(a)) and $\text{Cu}_{55}\text{Zr}_{40}\text{Sn}_5$ (Fig. 2(b)) ribbons consisted of a broad peak at $2\theta \approx 48.5^\circ$ with a width of 7.8° at half maximum and $2\theta \approx 48.2^\circ$ with a width of 8.2° at half maximum, respectively, indicating a single amorphous structure. The HRTEM image and the corresponding selected area diffraction pattern (SADP) for these alloys showed a featureless contrast and diffuse halo rings, respectively, a characteristic of single amorphous structure (not shown). Secondly, for detailed analysis on the local atomic structure, the SAXS profiles were obtained from as-spun $\text{Cu}_{55}\text{Zr}_{40}\text{Sn}_5$ ribbon in (b) as-quenched state and after annealing up to: (c) $793\ \text{K}$ and (d) $812\ \text{K}$ as shown in Fig. 3. The particle size can be determined from the low q region, which is called the Guinier region [11,12]. In this q region, the scattering profiles are described as:

$$I(q) = I(0) \exp \left\{ \frac{-R_g^2 q^2}{3} \right\} \quad (1)$$

where R_g is called the radius of gyration. For the system that includes the mono-disperse particles, $I(0)$ can be described as $nV^2(\rho - \rho_0)^2$ (n is the number of particles, V is the volume of the particle). Taking the natural logarithm of Eq. (1), we obtain

$$\ln I(q) = \ln I(0) - \left(\frac{R_g^2 q^2}{3} \right) \quad (2)$$

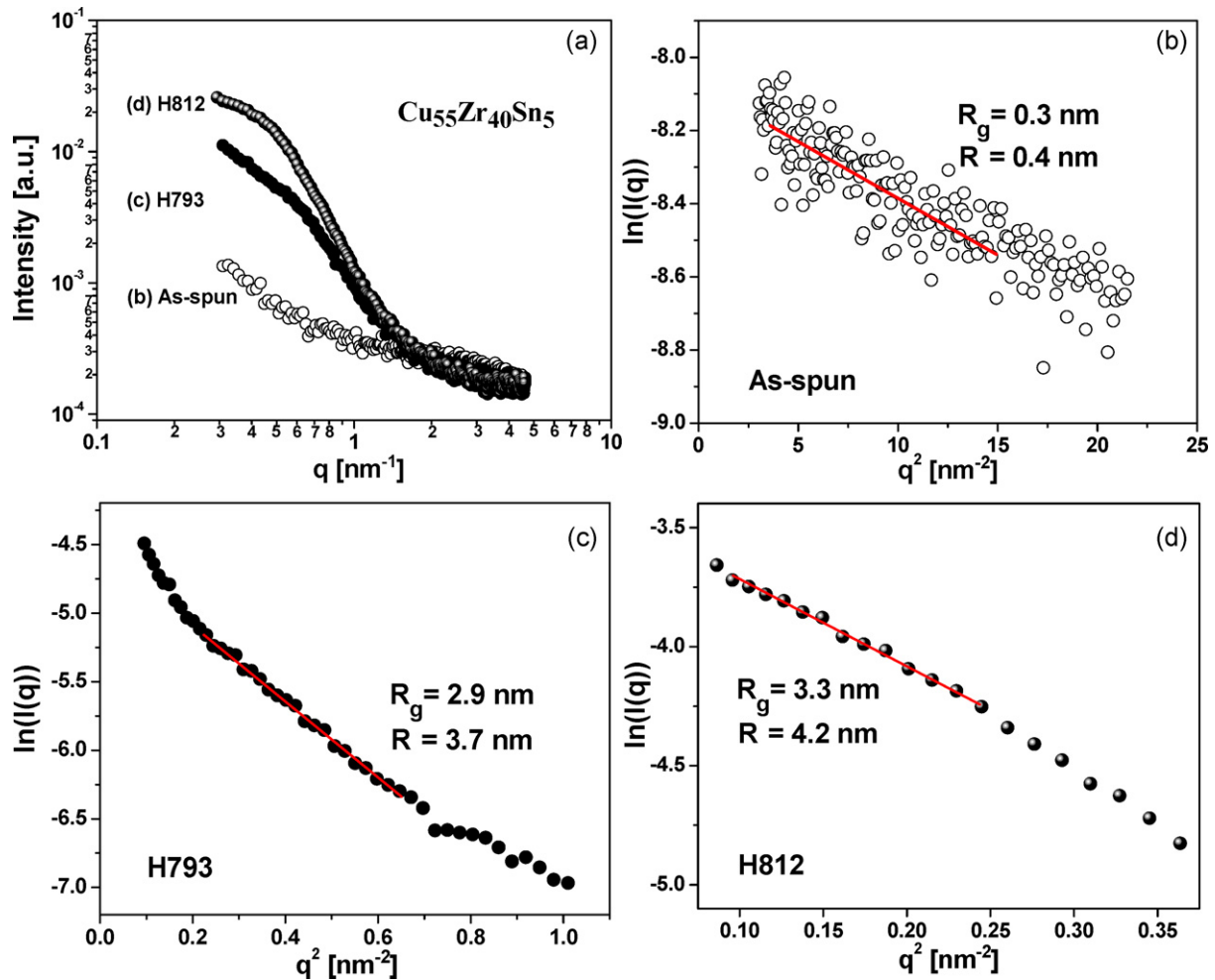


Fig. 3. SAXS profiles obtained from as-spun $\text{Cu}_{55}\text{Zr}_{40}\text{Sn}_5$ ribbon in (b) as-quenched state and after annealing up to: (c) 793 K and (d) 812 K.

Therefore, the value of R_g can be readily determined from the gradient of the linear region in the $\ln I(q) - q^2$ plot as shown in Fig. 3(b–d). In the case of spherical particles, the average particle radius r is $r = \sqrt{5/3}R_g$. From the SAXS results, it can be realized that the as-spun ribbon includes quenched-in nuclei in the amorphous matrix. In detail, the profiles in Fig. 3(a) indicate the q -range for background part and the scattering from nuclei. The background part ($q < 0.7 \text{ nm}^{-1}$, featureless decreasing part) is included in all samples, but it is too weak to see for others except as-spun ribbon. And the intensity in as-spun ribbon changes in high q -range larger than 1 nm^{-1} . Because the intensity becomes weak by annealing, we can conclude that the scattering for as-spun ribbon in this q -range is due to the quenched-in nuclei. Otherwise, it is difficult to conclude whether it is background or not. The nucleus seems to survive up to the 1st stage (the first crystallization), but does not exist in the sample heated to the 2nd stage (the second crystallization). Thus, the Guinier region of the sample annealed to 793 K is very much distorted from that expected for spherical particles, while in the sample annealed to 812 K, the Guinier region clearly appears. Assuming a spherical shape for the nanometer particles, the initial size of quenched-in nuclei in the as-spun ribbon ($q > 1 \text{ nm}^{-1}$) is 0.4 nm near the limitation value of the resolution in SAXS analysis. The particles grew up during the first exothermic reaction up to 3.7 nm. And then the nanometer particle disappeared during the second exothermic reaction due to the polymorphous crystallization of the Cu–Zr rich amorphous phase, which results in a coarse microstructure. This result can be con-

firmed by isothermal DSC measurements at 765 K. The DSC trace shows that the initial sharp decrease in heat release with time intervals of several minutes corresponds to growth of quenched-in nuclei, while the subsequent exothermic peak is related to the polymorphous crystallization of the Cu–Zr rich amorphous phase (not shown).

We found that in case of Cu–Zr metallic glass with 5 at.% Sn, although the alloy did not show an endothermic reaction related with SCLR before the 1st crystallization, a unique endothermic reaction between the first and the second exothermic peak was observed. This result may be attributed to the overlap of the exothermic reaction for the growth of the clusters in the SCLR of the Cu–Zr-rich amorphous phase. Fig. 4 shows a schematic Time–Temperature–Transformation (TTT) diagram displaying the path for the formation of the amorphous phase and quenched-in nuclei [13]. Fig. 4 suggests that the quenched-in nuclei in Cu–Zr–Sn alloy can form during solidification from the liquid state and/or during annealing from the single amorphous phase, which depends on alloy composition as well as cooling rate. By the addition of Sn to binary Cu–Zr BMGs, the large negative heat of mixing relationship between Zr and Sn (inset of Fig. 4) causes to strong affinity, which results in a new dominant crystallization behavior related to the formation of Zr–Sn intermediate phase. With an increase in Sn content, the negative heat of mixing and the diffusional asymmetry by the large size difference among constituent elements are favorable to the formation of an atomic scale cluster during solidification near the nose of TTT curve (Fig. 4(a and b)). In fact, the

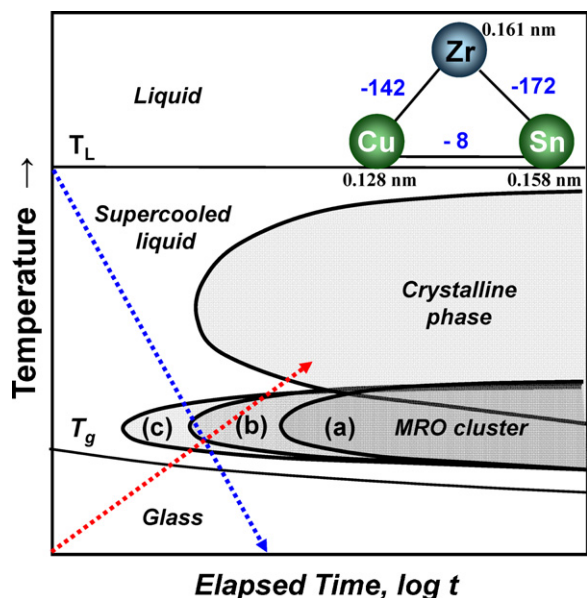


Fig. 4. Schematic Time–Temperature–Transformation (TTT) diagram showing the path for the formation of amorphous phase and MRO clusters. Insert figure shows Gold-schmidt radii and relationship of heat of fusion among constituent elements in Cu–Zr–Sn alloy system.

existence of icosahedral-like clusters even in binary Cu–Zr BMGs has been verified experimentally and theoretically [14,15]. In particular, the crystalline nuclei embedded in the amorphous matrix are under internal tension because the volume of the crystalline phase is much smaller than that of the amorphous phase. Thus, the application of thermal energy relieves this residual tensile stress endured by the crystalline nuclei, which stabilizes the crystalline nuclei and results in an easy growth of the clusters or acts as a nucleation site during heating in SCLR (Fig. 1B) [16–18]. Hence, the formation of an exothermic peak due to the MRO clustering in SCLR along with the endothermic T_g can explain the additional features observed in the DSC curve of amorphous $\text{Cu}_{50}\text{Zr}_{45}\text{Sn}_5$ ribbons. And a further addition of Sn results in crystallization during solidification (Fig. 4(c)), which deteriorates the glass-forming ability of the alloy system. Therefore, it can be understood that the addition of an element with large negative enthalpy of mixing and large size mismatch may cause to an atomic/nanometer scale clustering even during rapid quenching, and then this cluster can easily grow during heating in SCLR. Indeed, this exothermic reaction definitely results in abnormal endothermic reaction of SCLR in metallic glasses.

4. Conclusion

The present study reports the effect of Sn addition on unusual glass transition behavior in Cu–Zr BMGs. The anomalous glass transition behavior in $\text{Cu}_{55}\text{Zr}_{40}\text{Sn}_5$ ribbon can originate from the growth reaction of quenched-in nuclei (~ 0.4 nm) in the SCLR, which is closely related to strong affinity (Zr–Sn: -172 kJ/mol) and large size mismatch among constituent elements. The particles grew during the first exothermic reaction up to 3.7 nm. And then the nanometer particle disappeared during the second exothermic reaction due to the polymorphous crystallization of the Cu–Zr rich amorphous phase. We believe that the present approach for SCLR manipulation may be of use in the synthesis of a novel composite structure with uniform atomic/nanometer scale heterogeneity modulated by controlling cooling rate as well as by tailoring alloy composition.

Acknowledgements

This work was supported by the Global Research Laboratory Program of the Korean Ministry of Science. One of the authors (E.S. Park) was supported by a grant from the Fundamental R&D Program for Core Technology of Materials funded by the Ministry of Knowledge Economy, Republic of Korea. The authors are indebted to Dr. B.S. Seong at KAERI for performing the HRND experiment, Prof. K. Hono at NIMS, Japan for the SAXS experiment, and Prof. Frans Spaepen at Harvard University for thoughtful advice.

References

- [1] A.L. Greer, *Science* 267 (1995) 1947–1953.
- [2] T. Ichitsubo, E. Matsubara, H. Numakura, K. Tanaka, N. Nishiyama, R. Tarumi, *Phys. Rev. B* 72 (2005) 052201.
- [3] A.A. Kündig, M. Ohnuma, H.H. Ping, T. Ohkubo, K. Hono, *Acta Mater.* 52 (2004) 2441–2448.
- [4] E.S. Park, D.H. Kim, *Acta Mater.* 54 (2006) 2597–2604.
- [5] E.S. Park, E.Y. Jeong, J.-K. Lee, J.C. Bae, A.R. Kwon, A. Gebert, L. Schultz, H.J. Chang, D.H. Kim, *Scripta Mater.* 56 (2007) 197–200.
- [6] N. Mattern, T. Gemming, G. Goerigk, J. Eckert, *Scripta Mater.* 57 (2007) 29–32.
- [7] E.S. Park, H.J. Chang, D.H. Kim, *Acta Mater.* 56 (2008) 3120–3131.
- [8] E.S. Park, J.H. Na, D.H. Kim, *J. Appl. Phys.* 108 (2010) 053515.
- [9] A. Inoue, W. Zhang, *Mater. Trans.* 43 (2002) 2921–2925.
- [10] W. Zhang, A. Inoue, *J. Mater. Res.* 21 (2006) 234–241.
- [11] A. Guinier, G. Fournet, *Small-Angle Scattering of X-rays*, Wiley, New York, 1955.
- [12] K. Hono, M. Ohnuma, in: H.S. Nalwa (Ed.), *Magnetic nanostructure*, American Scientific Publisher, Stevenson Ranch, CA, 2002.
- [13] C.A. Angell, *MRS Bull.* 33 (2008) 544–555.
- [14] X.D. Wang, S. Yin, Q.P. Cao, J.Z. Jiang, H. Franz, Z.H. Jin, *Appl. Phys. Lett.* 92 (2008) 011902.
- [15] Y.Q. Cheng, A.J. Cao, H.W. Sheng, E. Ma, *Acta Mater.* 56 (2008) 5263–5275.
- [16] A.P. Tsai, T. Kamiyama, Y. Kawamura, A. Inoue, T. Masumoto, *Acta Mater.* 45 (1997) 1477–1487.
- [17] D.R. Allen, J.C. Foley, J.H. Perepezko, *Acta Mater.* 46 (1997) 431–440.
- [18] T. Gloriant, D.H. Ping, K. Hono, A.L. Greer, M.D. Baró, *Mater. Sci. Eng. A* 304–306 (2001) 315–320.